ChemComm

COMMUNICATION

View Article Online
View Journal

Cite this: DOI: 10.1039/d6cc01011c

Received 15th February 2026,
Accepted 12th March 2026

DOI: 10.1039/d6cc01011c

rsc.li/chemcomm

Backbone deprotonation defines a hidden decomposition pathway of diphosphine ligands

Logan J. Taylor, A. Dina Dilinaer, Paul D. Boyle and Marcus W. Drover *

Diphosphine ligands are ubiquitous partners in synthetic chemistry, enabling tuneable reactivity and selectivity. Here, we identify an overlooked decomposition pathway: base-induced deprotonation of an ethylene diphosphine carbon backbone to give a strained metallabicycle. The instability of this scaffold, reflected in a short half-life and decomposition even during routine filtration, has implications for diphosphine–metal coordination chemistry and catalysis under basic conditions.

Ligand design is a cornerstone of molecular coordination chemistry, providing a means to stabilize s, p, d, and even f-block metal complexes.[1,2] Amongst possible candidates, diphosphine ligands, comprising two phosphine donors linked intramolecularly, have been extensively studied. Both phosphine substituents and ligand backbone are tunable, allowing for variability in length, rigidity, and shape (*i.e.*, aliphatic, aromatic, *etc.*) (Scheme 1a).[3,4] Beyond their primary coordination role, diphosphines can serve as templates for the introduction of secondary coordination sphere (SCS) elements[5] or point, axial, or other forms of chirality.[6–8]

Although often considered spectator ligands, diphosphines can undergo unproductive reactivity, including nucleophilic attack on metal-bound substrates[9] or activation of its ligand C–H bonds.[10] Larger diphosphine chelates can form cyclic structures upon heating or on exposure to external reagents.[11–17] For example, Fogg and co-workers showed that a butylene-linked diphosphine Ru complex reacted with excess silylene ligand to give a [3.5] ruthenacycle (where [*n.m*] denotes fused *n*- and *m*- membered rings).[12] Trovitch and co-workers reported that heating a tetradentate Fe-[*P*,*N*,*N*,*P*] complex led to benzene elimination and formation of a [5.3] cycle (Scheme 1b, left),[13] while Lacy and colleagues observed that deprotonation of a Ru-[*P*,*N*] complex gave rise to a unique κ^3-*N*,*C*,*P* bound Ru complex having a [3.4] cycle, which was reactive toward H_2.[14] Intricate knowledge of these reactive pathways underpins application of such ligands in catalysis.

Department of Chemistry, Western University, 1151 Richmond Street, London, ON N8K 3G6, Canada. E-mail: marcus.drover@uwo.ca

As part of our ongoing research program, we have explored diphosphine ligands as anchoring points for the introduction of pendent Lewis acid functionality, reporting scaffolds bearing one,[18,19] two,[20] and even four[21,22] Lewis acid group(s). We have also studied diphosphine ligands in a purely supporting role, reporting the first example of a room-temperature stable iron "tucked-in" complex, formed by treatment of [Cp*Fe(diphosphine)(N_2)]$^+$ with base (Scheme 1b, right).[23] In this reaction, deprotonation of a peripheral Cp(CH_3) group generates a direct {Fe–CH_2} bonding interaction.[23] This reactive Cp*Fe 'tucked-in' complex exhibits high nucleophilicity, undergoing hydroboration, for example, to form a pendent {Cp*CH_2BCy_2} fragment – an underexploited site for secondary coordination sphere manipulation – which we leveraged for CO_2 dihydroboration.[24]

To further understand the factors governing tucked-in formation in [{Cp^R}Fe(diphosphine)]$^+$ (R = functionalized Cp)

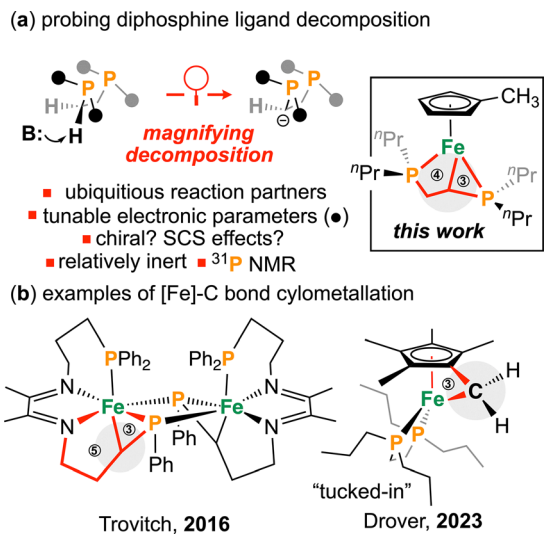

Scheme 1 (a) Probing diphosphine decomposition space, SCS = secondary coordination sphere; (b) examples of cycometallated Fe–C complexes. Circles with numbers refer to ring size.

complexes, we were interested in exploring the chemistry of a related analogue, Cp^{Me}, containing a single methylated site. Reactivity of a {Cp^{Me}}Fe complex with base, however, did not produce the expected tucked-in iron complex. Instead, in the case of [{Cp^{Me}}Fe(diphosphine)(Cl)], deprotonation occurred at the diphosphine backbone, rather than the Cp^{Me} group, producing a strained [3.4] ferracycle (Scheme 1a, right). This reactive complex represents, to our knowledge, the first characterized coordination compound featuring a strained κ^3-*P*,*C*,*P* ethylene-bridged diphosphine motif. These findings highlight a possible unrecognized decomposition pathway and raise questions about the compatibility of widely used diphosphine ligands with nucleophilic bases.

To begin, a THF slurry of sodium methylcyclopentadienide ($NaCp^{Me}$)[25] was reacted with [Fe^{II}(d*n*ppe)$_2$(Cl)$_2$] (d*n*ppe = 1,2-bis(di-*n*-propylphosphino)ethane) to give [{Cp^{Me}}Fe(d*n*ppe)(Cl)] (**1**), with concomitant release of one equivalent of free d*n*ppe ligand. The $^{31}P\{^1H\}$ NMR spectrum showed a single resonance at δ_P = 89.2 ppm, approximately 10 ppm downfield of the [Cp*Fe(dnppe)(Cl)] analogue (Scheme 2). ^{1}H NMR spectroscopy revealed C_s symmetry, with two singlets at δ_H = 4.59 and 2.66 ppm; 2D ^{1}H–^{13}C HMBC and ^{1}H–^{1}H COSY NMR spectroscopic experiments confirmed that these signals correspond to the Cp–H protons. Dissolution of **1** in hexanes and storing the saturated solution at −35 °C overnight afforded purple-brown crystals suitable for X-ray diffraction (Fig. 1, left).

We next investigated **1** as a potential precursor to a tucked-in complex, which was expected to give a single ^{31}P NMR spectral resonance. Treatment of **1** with 3 equiv. of *n*-BuLi at −35 °C and analysis of the crude reaction mixture by $^{31}P\{^1H\}$ NMR spectroscopy, however, indicated formation of at least three new diamagnetic compounds: signals at δ_P = 102.8 and 97.5 ppm along with a pair of 'roofed' [AB] doublets at δ_P = 1.65 and −1.22 ppm ($J_{P,P}$ = 32.2 Hz) in a 3 : 1 : 2.5 ratio (Scheme 2). The signals at δ_P = 102.8 and 97.5 ppm were assigned as side products arising from *n*-BuLi attack at iron: [{Cp^{Me}}Fe(d*n*ppe)(^{n}Bu)] (**2**) and its β-hydride elimination product, [{Cp^{Me}}Fe(d*n*ppe)(H)] (**3**), respectively, indicating that the targeted tucked-in Cp^{Me}Fe complex was not prepared. ^{1}H–^{31}P HMBC NMR spectroscopy confirmed the assignment of **2** with the signal at δ_P = 97.5 ppm correlating to a ^{1}H NMR signal at δ_H = −0.24 ppm; 1D ^{1}H TOCSY NMR linked this site to three others, consistent with an {Fe-*n*-Bu} fragment. The most downfield peak at δ_P = 102.8 ppm corresponds to the iron(II)-hydride, **3**, which was independently prepared by reaction of **1** with *t*-BuLi. Additional support for the structure of **3** comes from a phosphorus-coupled triplet at δ_H = −17.3 ppm ($^2J_{P,H}$ = 72.3 Hz) and a broad Fe—H stretch in the FT-IR ATR spectrum ($\nu_{Fe,H}$ = 1830 cm^{-1}). A molecular ion of the appropriate exact mass and isotope pattern was also observed for complexes **2** (*m*/*z* = 454.258) and **3** (*m*/*z* = 398.195) by liquid injection field desorption ionization mass spectrometry (LIFDI-HRMS).[26]

We next sought to identify the species responsible for the ^{31}P NMR signals at δ_P = 1.65 and −1.22 ppm, which we hypothesized arose from complex **4**, formed *via* direct C–H deprotonation rather than Fe–Cl attack (Scheme 2). Reaction of [{Cp^{Me}}Fe(d*n*ppe)(Cl)] (**1**) with *n*-BuLi at lower temperature (−78 °C) afforded a deep red solution, predominantly containing the new product **4** in 90% by quantitative ^{31}P NMR spectroscopy. ^{1}H NMR spectroscopy of **4** revealed four Cp—H resonances, consistent with a C_1-symmetric molecule, along with a distinctive upfield signal at δ_H = −0.14 ppm, which was responsive to ^{31}P decoupling. A 1D ^{1}H TOCSY experiment showed coupling to partners at δ_H = 2.17 and 2.82 ppm, whose spin system was appropriately modelled (Fig. 2a and b). ^{1}H–^{31}P HMBC correlations identified these protons as having a long-range correlation with the diphosphine phosphorus signals at δ_P = 1.65 and −1.22 ppm. ^{1}H–^{13}C HSQC NMR spectroscopy further indicated that the resonances at δ_H = 2.17 and 2.82 ppm were geminal (on the same carbon), while the third proton was strongly upfield shifted (δ_C = −25.1 ppm). This is contrasted with [Cp*Fe(d*n*ppe)(CH$_3$)], for example, which has a ^{13}C NMR

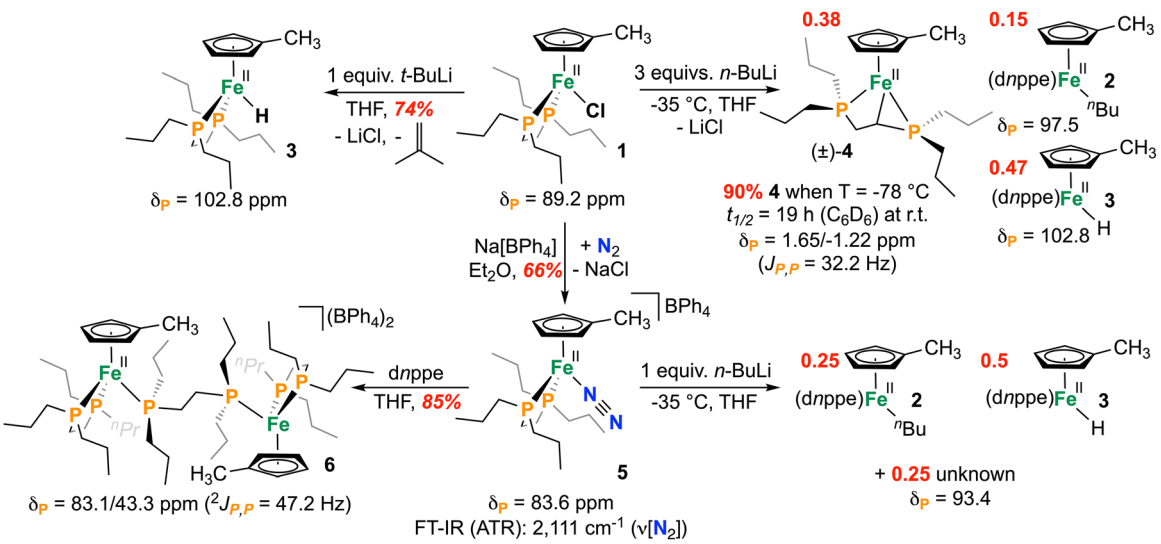

Scheme 2 Synthetic pathway of the formation of **4** and additional products.

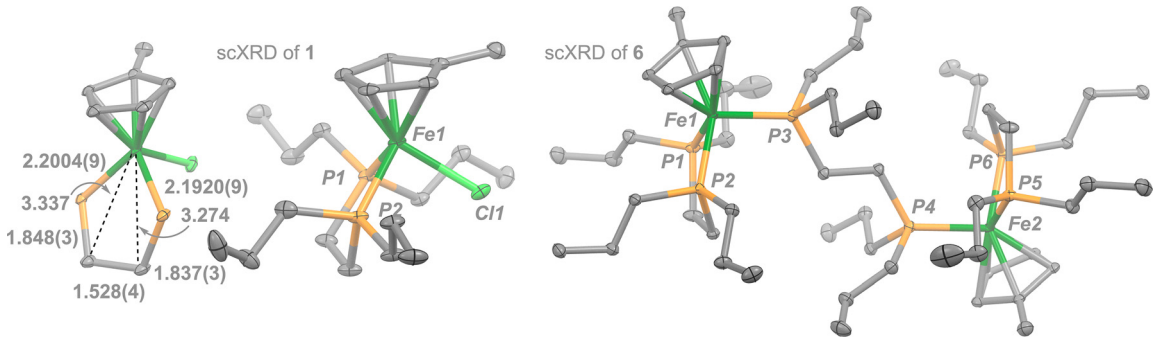

Fig. 1 Solid-state structure of **1** and **6** with an enhanced view of the Fe-diphosphine core of **1** (left) (ellipsoids drawn at 50% probability; hydrogen atoms and d*n*ppe ^{n}Pr groups have been omitted for clarity).

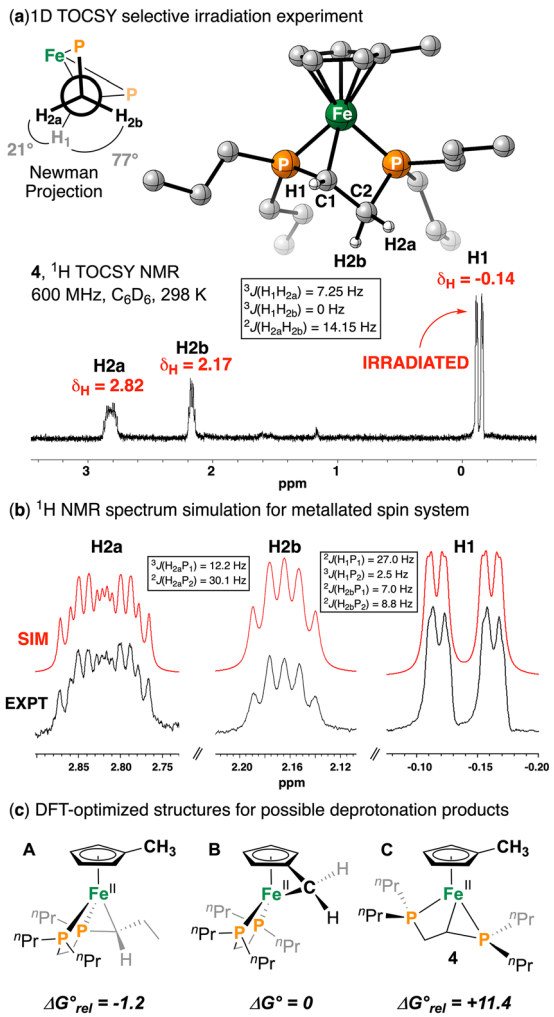

Fig. 2 (a) 1D ^{1}H TOCSY NMR (600 MHz, C_6D_6, 298 K) of **4**, inset shows DFT-optimized structure; (b) ^{1}H NMR spectrum simulation for metalated spin system of **4**, sim = simulation, expt = experimental data; (c) DFT optimized structures and calculated relative free energies in kcal mol^{-1}.

signal at δ_C = −11.3 ($^{2}J_{P,C}$ = 24.1 Hz).[21] Taken together, these data are consistent with deprotonation of the diphosphine ligand backbone to form a strained [4.3] ferracycle, [{Cp^{Me}}Fe(κ^{3}-*P*,*C*,*P*-d*n*ppe)] (**4**). Complex **4** was also examined using LIFDI-HRMS, providing a molecular ion at *m*/*z* = 396.179, accompanied by an overlapping $[M + H]^+$ pattern at *m*/*z* = 397.187 in a 2 : 3 ratio.[27] To our knowledge, this represents the first observed example of backbone deprotonation at a coordinated ethylene-bridged diphosphine ligand. This outcome also provides an interesting contrast between *n*-BuLi and *t*-BuLi reactivity: although attack at iron is observed in both cases, *n*-BuLi generates Fe–^{n}Bu (**2**), Fe–H (**3**), and **4**, whereas *t*-BuLi produces only the iron hydride **2**. The behaviour of the latter is consistent with *t*-BuLi being too sterically demanding to access the backbone carbon, precluding deprotonation and thus formation of **4**.

Attempts to obtain crystalline **4** suitable for single crystal X-ray diffraction were not met with success. Consistent with its strained [{Cp^{Me}}Fe(κ^{3}-*P*,*C*,*P*-d*n*ppe)] core, complex **4** decomposes rapidly upon contact with common filter media such as Celite® 545, as well as in solution or in the solid-state at room temperature or even at −35 °C. Using an internal standard and ^{31}P{^{1}H} NMR spectroscopy in C_6D_6, gradual decay was observed, yielding a half-life of $t_{1/2} \approx 19$ h at 25 °C.

A computational model of **4** revealed a strained three-legged piano stool geometry with κ^{3}-*P*,*C*,*P* diphosphine ligand coordination (Fig. 2a, inset). The Fe–C bond is shortened to 2.070 Å compared to 2.131(1) Å in the related [Cp*Fe(d*n*ppe)(CH$_3$)][21] complex. Similarly, the Fe–P bonds contract to 2.156 and 2.137 Å, relative to 2.162(4) and 2.180(4) Å in [Cp*Fe(d*n*ppe)(CH$_3$)],[21] consistent with the effects of κ^{3}-coordination. The reaction of **1** with *n*-BuLi can, in principle, yield deprotonation at three sites: (a) an *n*-Pr arm; (b) the diphosphine backbone; or (c) the Cp^{Me} ligand, with 8H:4H:3H probability. Compared to tucked-in complex **B** (Fig. 2c), complex **4** (**C**) is calculated to be 11.4 kcal mol^{-1} higher in energy, whereas deprotonation at the *n*-Pr(CH$_2$) arm (**A**) is slightly more stable by 1.2 kcal mol^{-1}.[23] This indicates that **4** forms as a kinetic product, which is consistent with its clean formation at low temperature and limited stability. NMR chemical shifts were also obtained using DFT calculations. As described previously, cyclometallation of phosphine ligands typically generates small chelate rings, leading to ^{31}P resonances 50–100 ppm upfield of the precursor.[28] This is observed here: δ_P = 89.2 ppm for **1** *vs.* δ_P = 1.65 and −1.22 ppm for **4** ($\Delta\delta_P \sim 90$ ppm). Using optimized structures from DFT (see SI), calculated ^{31}P chemical shifts reproduce this trend, giving

$\Delta\delta_P \approx 99$ ppm, once again supporting the assignment of **4** as a diphosphine-backbone-deprotonated species.

To determine whether **4** can arise from precursors other than [{Cp^{Me}}Fe(d*n*ppe)(Cl)] (**1**), we targeted the alternative halide-free complex [{Cp^{Me}}Fe(d*n*ppe)(N$_2$)]BPh$_4$ (**5**), which for the related Cp* complex, was required for clean tucked-in complex preparation.[23] Initial attempts combining [Fe^{II}(d*n*ppe)$_2$(Cl)$_2$], NaCp^{Me}, and NaBPh$_4$, however, were unsuccessful, as released d*n*ppe was trapped to provide the μ-bridged complex **6**. Complex **6** was characterized by single crystal X-ray diffraction (Fig. 1, right), HRESI-MS, and $^{31}P\{^1H\}$ NMR spectroscopy, which showed a doublet and quartet at δ_P = 83.1 and 43.3 ppm ($^2J_{P,P}$ = 47.2 Hz) (Scheme 2). This outcome suggests reactivity from the desired complex [{Cp^{Me}}Fe(d*n*ppe)(N$_2$)]$^+$. Of note, μ-d*n*ppe coordination is not observed for the Cp* analogue, likely due to the more electron-poor iron centre and/or reduced steric bulk of the Cp^{Me} system in **5**. By carefully omitting exogenous phosphine and reacting **1** with NaBPh$_4$, the desired [{Cp^{Me}}Fe(d*n*ppe)(N$_2$)]$^+$ (**5**) was obtained, exhibiting a single $^{31}P\{^1H\}$ NMR resonance at δ_P = 83.6 ppm and an FT-IR N$_2$ stretch of 2111 cm^{-1}. By HRESI-MS, a strong [M–N$_2$]$^+$ peak at *m*/*z* = 397.187 was also observed.

Unlike the Fe–Cl complex **1**, the [Fe–N$_2$]$^+$ cation **5** does not form the cyclometallated product **4**. Reaction of **5** with 3 equiv. *n*-BuLi at −35 °C gave a $^{31}P\{^1H\}$ NMR spectrum, exhibiting three signals in a roughly 1 : 2 : 1 ratio, assigned as **2**, **3** and a previously unobserved singlet at δ_P = 93.4 ppm, whose identity remains unknown (Scheme 2). Conducting the reaction at −78 °C likewise failed to generate **4** (see SI). Further differences between Cp* and the Cp^{Me} systems emerged upon treatment of [Cp*Fe(d*n*ppe)(Cl)] with *n*-BuLi at −78 °C. This reaction also generated a product consistent with an Fe-κ^3-*P*,*C*,*P*-d*n*ppe coordination mode, however, in this case the Fe ''tucked-in'' complex is formed preferentially (Scheme 1b, right; see SI for details). These observations underscore a fundamental distinction between the Cp^{Me} and Cp* platforms. Under comparable conditions, the tucked-in product is more readily accessed in the Cp*Fe system, likely reflecting the greater number of methyl C–H sites available for deprotonation (five-fold higher relative to Cp^{Me}). Nevertheless, the κ^3-*P*,*C*,*P* coordination motif is common to both systems, highlighting the general accessibility of this binding mode across the two ligand environments.

We have identified that treatment of [{Cp^{Me}}Fe(d*n*ppe)(Cl)] (**1**) with base results in deprotonation of the diphosphine ligand backbone, affording a strained κ^3-*P*,*C*,*P* Fe iron complex (**4**). Combined spectroscopic and computational analyses reveal its unusual structure and intrinsic instability and point to a potential phosphine decomposition pathway that may warrant consideration when evaluating the reactivity of metal–diphosphine systems under basic conditions.

The authors are grateful to Western University, the Council of Ontario Universities for a John C. Polanyi award to M. W. D., the Canadian Foundation for Innovation (LOF-212442), the Natural Sciences and Engineering Research Council of Canada (Discovery Grant, RGPIN-2020-04480 (M. W. D.), Discovery Launch Supplement, DGECR-2020-00183), and graduate award (CGRS-M to L. J. T.) for funding. The authors also thank Mr Quentin Lepeintre for initial synthesis of NaCp^{Me} and Dr Mathew Willans for assistance in the simulation of ^{1}H NMR spectral data.

Conflicts of interest

There are no conflicts to declare.

Data availability

The data supporting this article have been included as part of the supplementary information (SI). Supplementary information is available. See DOI: https://doi.org/10.1039/d6cc01011c.

CCDC 2527971 (**1**) and 2527972 (**6**) contain the supplementary crystallographic data for this paper.[29a,b]

References

1 P. Dierkes and P. W. N. M. van Leeuwen, *J. Chem. Soc., Dalton Trans.*, 1999, 1519–1530.
2 H. Shet, U. Parmar, S. Bhilare and A. R. Kapdi, *Org. Chem. Front.*, 2021, **8**, 1599–1656.
3 D. Zhao, T. M. Neubauer and B. L. Feringa, *Nat. Commun.*, 2015, **6**, 6652.
4 E. S. Wiendner, A. M. Appel, S. Raugei, W. J. Shaw and R. M. Bullock, *Chem. Rev.*, 2022, **122**, 12427–12474.
5 M. W. Drover, *Chem. Soc. Rev.*, 2022, **51**, 1861–1880.
6 T. Benincori, E. Brenna, F. Sannicolo, L. Trimarco, P. Antongnazza, E. Cesarotti, F. Demartin and T. Pilati, *J. Org. Chem.*, 1996, **61**, 6244–6251.
7 F. Zhang, G.-Q. Chen and X. Zhang, *Org. Lett.*, 2024, **26**, 1623–1628.
8 T. Saito, T. Yokozawa, T. Ishizaki, T. Moroi, N. Sayo, T. Miura and H. Kumobayashi, *Adv. Synth. Catal.*, 2001, **343**, 264–267.
9 S. Aghazada, D. Munz, F. W. Heinemann, A. Scheurer and K. Meyer, *J. Am. Chem. Soc.*, 2021, **143**, 17219–17225.
10 T. Ikariya and A. Yamamoto, *J. Organomet. Chem.*, 1976, **118**, 65–77.
11 T. Simler, G. Frison, P. Braunstein and A. A. Danopoulos, *Dalton Trans.*, 2016, **45**, 2800–2804.
12 D. Amoroso, M. Haaf, G. P. A. Yap, R. West and D. E. Fogg, *Organometallics*, 2002, **21**, 534–540.
13 C. Ghosh, T. L. Groy, A. C. Bowman and R. J. Trovitch, *Chem. Commun.*, 2016, **52**, 4552.
14 P. M. Fanara, V. Vigneswaran, P. S. Gunasekera, S. N. MacMillan and D. C. Lacy, *Organometallics*, 2022, **41**, 93–98.
15 L. S. Merz, H. Wadepohl, E. Clot and L. H. Gade, *Chem. Sci.*, 2018, **9**, 5223–5232.
16 X. Ye, P. N. Plessow, M. K. Brinks, M. Schelwies, T. Schaub, F. Rominger, R. Paciello, M. Limbach and P. Hofmann, *J. Am. Chem. Soc.*, 2014, **136**, 5923–592915.
17 R. Beck, U. Flörke and H. F. Klein, *Organometallics*, 2015, **34**, 1454–1464.
18 J. A. Zurakowski, B. J. H. Austen, K. R. Brown and M. W. Drover, *Chem. Commun.*, 2022, **58**, 2500–2503.
19 M. L. Clapson, H. Sharma, J. A. Zurakowski and M. W. Drover, *Chem. – Eur. J.*, 2023, **29**, e202203763.
20 B. J. H. Austen, H. Sharma, J. A. Zurakowski and M. W. Drover, *Organometallics*, 2022, **41**, 2709–2715.
21 J. A. Zurakowski, K. R. Brown and M. W. Drover, *Inorg. Chem.*, 2023, **62**, 7053–7060.
22 J. A. Zurakowski, M. Bhattacharyya, D. M. Spasyuk and M. W. Drover, *Inorg. Chem.*, 2020, **60**, 37–41.
23 J. A. Zurakowski and M. W. Drover, *Chem. Commun.*, 2023, **59**, 11349–11352.

24 C. S. Durfy, J. A. Zurakowski and M. W. Drover, *Angew. Chem., Int. Ed.*, 2025, **64**, e202421599.
25 E. J. Palmer, R. J. Strittmatter, K. T. Thornley, J. C. Gallucci and B. E. Bursten, *Polyhedron*, 2013, **58**, 120–128.
26 M. Muhr, P. Heiss, M. Schutz, R. Buhler, C. Gemel, M. H. Linden, H. B. Linden and R. A. Fischer, *Dalton Trans.*, 2021, **50**, 9031–9036.
27 J. H. Gross, *Eur. J. Mass Spectrom.*, 2020, **26**, 241–273.
28 P. E. Garrou, *Chem. Rev.*, 1981, **81**, 229–266.
29 (*a*) CCDC 2527971: Experimental Crystal Structure Determination, 2026, DOI: 10.5517/ccdc.csd.cc2qvkgm; (*b*) CCDC 2527972: Experimental Crystal Structure Determination, 2026, DOI: 10.5517/ccdc.csd.cc2qvkhn.